The aryl hydrocarbon receptor suppresses immunity to oral squamous cell carcinoma through immune checkpoint regulation

Jessica E. Kenison[a], Zhongyan Wang[b], Kangkang Yang[b], Megan Snyder[c], Francisco J. Quintana[d,e], and David H. Sherr[a,b,c,1]

[a]Department of Pathology and Laboratory Medicine, Boston University School of Medicine, Boston, MA 02118; [b]Department of Environmental Health, Boston University School of Public Health, Boston, MA 02118; [c]Graduate Program in Genetics and Genomics, Boston University School of Medicine, Boston, MA 02118; [d]Ann Romney Center for Neurologic Diseases, Brigham and Women's Hospital, Harvard Medical School, Boston, MA 02115; and [e]The Broad Institute of MIT and Harvard, Cambridge, MA 02142

Edited by Gordon J. Freeman, Dana-Farber Cancer Institute and Harvard Medical School, Boston, MA, and accepted by Editorial Board Member Tadatsugu Taniguchi March 29, 2021 (received for review June 25, 2020)

Immune checkpoint inhibitors represent some of the most important cancer treatments developed in the last 20 y. However, existing immunotherapy approaches benefit only a minority of patients. Here, we provide evidence that the aryl hydrocarbon receptor (AhR) is a central player in the regulation of multiple immune checkpoints in oral squamous cell carcinoma (OSCC). Orthotopic transplant of mouse OSCC cells from which the AhR has been deleted ($MOC1^{AhR\text{-}KO}$) results, within 1 wk, in the growth of small tumors that are then completely rejected within 2 wk, concomitant with an increase in activated T cells in tumor-draining lymph nodes (tdLNs) and T cell signaling within the tumor. By 2 wk, AhR^{+} control cells ($MOC1^{Cas9}$), but not $MOC1^{AhR\text{-}KO}$ cells up-regulate exhaustion pathways in the tumor-infiltrating T cells and expression of checkpoint molecules on $CD4^{+}$ T cells (PD-1, CTLA4, Lag3, and CD39) and macrophages, dendritic cells, and $Ly6G^{+}$ myeloid cells (PD-L1 and CD39) in tdLNs. Notably, $MOC1^{AhR\text{-}KO}$ cell transplant renders mice 100% immune to later challenge with wild-type tumors. Analysis of altered signaling pathways within $MOC1^{AhR\text{-}KO}$ cells shows that the AhR controls baseline and IFNγ-induced *Ido* and PD-L1 expression, the latter of which occurs through direct transcriptional control. These observations 1) confirm the importance of malignant cell AhR in suppression of tumor immunity, 2) demonstrate the involvement of the AhR in IFNγ control of PD-L1 and IDO expression in the cancer context, and 3) suggest that the AhR is a viable target for modulation of multiple immune checkpoints.

aryl hydrocarbon receptor | oral squamous cell carcinoma | immune checkpoint | dioxin | environmental

Over 350,000 patients are diagnosed worldwide each year with head and neck squamous cell carcinoma (HNSCC) (1). Despite advances in surgery, chemotherapy, and radiation, all of which result in significant morbidity, more than 177,000 HNSCC patients die (2). Recent successes achieved by targeting immune checkpoint molecules like PD-1, PD-L1, and CTLA4 demonstrate that suppression of tumor-specific immunity plays a significant role in HNSCC pathology (3). However, complete and durable responses with immune checkpoint inhibitors are rare, and only a minority of HNSCC patients benefit (3, 4). Therefore, defining the mechanisms that drive antitumor immunosuppression in HNSCC is of great clinical importance.

The aryl hydrocarbon receptor (AhR) is the only ligand-activated member of the PER-ARNT-SIM (bHLH-PAS) superfamily of transcription factors (5). It is overexpressed and chronically active in HNSCC (6, 7), breast cancer (8–11), glioblastoma (12, 13), and other cancers (14–17). Chronically active AhR enhances cancer "stem-ness" and drives malignant cell migration, invasion, and metastasis (6, 7, 17, 18). Further, AhR expressed in tumors drives the expression of indoleamine 2,3-dioxygenase (IDO) and tryptophan 2,3-dioxygenase (TDO), which metabolize tryptophan into the immunosuppressive AhR agonist kynurenine. Several metabolites derived from kynurenine are also AhR ligands (11, 19, 20). Thus, the AhR participates in an AhR→IDO/TDO→AhR ligand amplification loop in which it promotes IDO and/or TDO expression and catalyzes the synthesis of immunosuppressive AhR agonists. These agonists may then modulate antitumor immune responses through AhR signaling in immune cells in the tumor microenvironment (TME). In support of this hypothesis, AhR signaling modulates adaptive immunity through its effects on T cells (21–24) and antigen-presenting cells (25–29). For example, glioblastoma-derived kynurenine drives tumor invasion (30) while it promotes the recruitment and differentiation of immunosuppressive tumor-associated macrophages (13). Kynurenine also induces PD-1 on tumor-infiltrating $CD8^{+}$ T cells (31), raising the possibility that AhR ligands produced by malignant cells through the AhR→IDO/TDO→Kyn amplification loop affect T cells in the TME (11). A complete understanding of the role of AhR signaling in tumor cells and the TME is lacking, however, and many questions remain.

To test the hypothesis that malignant cell AhR contributes to an immunosuppressive TME, we deleted AhR from murine oral cancer (MOC1 or MOC22) cells (32–34) and analyzed carcinoma

Significance

Immune checkpoint inhibitors have emerged as critical therapeutics for several cancer types, including head and neck squamous cell carcinoma. However, enthusiasm remains constrained by the fact that only a minority of patients benefit. Therefore, there is a need to identify new immunotherapy targets. Here, we provide evidence supporting our hypothesis that the aryl hydrocarbon receptor (AhR) influences multiple immune checkpoints in a model of oral squamous cell carcinoma (OSCC). Remarkably, transplant of AhR-deleted OSCC cells generates completely protective tumor immunity characterized by a decrease in multiple immune checkpoints (PD-L1, CD39, CTLA4, PD1, and Lag3) on malignant and/or immune cells. These results have important implications for understanding the biology of cancer immunosuppression and for targeting the AhR for cancer immunotherapy.

Author contributions: J.E.K., Z.W., F.J.Q., and D.H.S. designed research; J.E.K., Z.W., K.Y., and M.S. performed research; J.E.K. and Z.W. analyzed data; and J.E.K., F.J.Q., and D.H.S. wrote the paper.

Competing interest statement: J.E.K. and F.J.Q. report equity in AnTolRx, Inc.

This article is a PNAS Direct Submission. G.J.F. is a guest editor invited by the Editorial Board.

[1]To whom correspondence may be addressed. Email: dsherr@bu.edu.

This article contains supporting information online at https://www.pnas.org/lookup/suppl/doi:10.1073/pnas.2012692118/-/DCSupplemental.

Published May 3, 2021.

growth and tumor-specific immunity in vivo. Since studies with environmental AhR ligands (e.g., tobacco smoke) suggest interactions between the AhR and PD-L1 (35), and previous studies demonstrate AhR transcriptional control of CD39 expression (13), we also considered the possibility that malignant cell AhR contributes to immunosuppression via these or other important immune checkpoints.

Results

Validation of AhR Deletion from Oral Squamous Cell Carcinoma (OSCC). Our working hypothesis is that the AhR within malignant cells drives immunosuppression in the TME and that AhR deletion may break the amplification cycle, reverse immunosuppression, and result in tumor rejection. To test this hypothesis, we used a murine orthotopic (tongue) oral cancer (MOC) model, characterized by high MHC I expression, multiple neoantigens, and susceptibility to anti-PD-L1 checkpoint therapy (32, 33, 36).

AhR knockout through targeting of exon 1 ($MOC1^{AhR\text{-}KO}$ cells) was confirmed by Western blotting and by lack of response to the potent AhR ligand 6-formylindolo[3,2-b]carbazole (FICZ), as measured by an AhR-dependent reporter gene assay (*SI Appendix*, Fig. S1 *A* and *B*). Similarly, little or no *Cyp1a1* or *Cyp1b1*, prototypical AhR target genes, was detected in $MOC1^{AhR\text{-}KO}$ cells by qPCR in the presence or absence of FICZ (*SI Appendix*, Fig. S1*C*). As shown with human OSCC (6) and breast cancer (11, 18), $MOC1^{AhR\text{-}KO}$ cells exhibited impaired migration as compared with MOC1 wild-type ($MOC1^{WT}$) cells or $MOC1^{Cas9}$ control cells, which express Cas9 but no guide RNA (*SI Appendix*, Fig. S1 *D* and *E*). In agreement with our previous observations (6, 11, 18, 37), AhR deletion did not affect MOC1 cell proliferation in vitro (*SI Appendix*, Fig. S1*F*). These studies show that the AhR controls OSCC migration, but not growth or viability in vitro.

AhR Expression in MOC1 Cells Is Required for Sustained In Vivo Orthotopic Tumor Growth. To evaluate the effect that AhR expression in tumor cells has on the establishment of an immunosuppressive TME, we injected 3×10^5 $MOC1^{AhR\text{-}KO}$ or control $MOC1^{Cas9}$ cells into the center of tongues from C57BL/6J mice. Both $MOC1^{AhR\text{-}KO}$ and $MOC1^{Cas9}$ cells generated small tumors within 7 d (Fig. 1 *A*, *Left* and Fig. 1*B*). However, the tumors generated with $MOC1^{AhR\text{-}KO}$ cells completely disappeared by week 2 and no further growth was observed over a 7-wk period (Fig. 1 *A*, *Right* and Fig. 1*B*).

We postulated that the rapid clearance of the tumor cells in the $MOC1^{AhR\text{-}KO}$-injected mice reflects a robust immune response to $MOC1^{AhR\text{-}KO}$ cells. To test this hypothesis, we injected $MOC1^{Cas9}$ or $MOC1^{AhR\text{-}KO}$ cells into the tongues of nonobese diabetic/severe combined immunodeficient (NOD/SCID) mice (Fig. 1*C*). $MOC1^{Cas9}$ tumors grew faster in NOD/SCID than in C57BL/6 mice (compare Fig. 1 *A* and *C*), a result consistent with a significant contribution of the immune system to slowing OSCC growth. $MOC1^{AhR\text{-}KO}$ cells grew at the same rate as $MOC1^{Cas9}$ cells in NOD/SCID mice (Fig. 1*C*), indicating that $MOC1^{AhR\text{-}KO}$ cells are not inherently growth defective and that the immune compartment is important for $MOC1^{AhR\text{-}KO}$ tumor growth suppression.

To determine the mechanism(s) responsible for tumor growth inhibition, we investigated the transcriptional profile of the tumor environment using the 770-gene set NanoString PanCancer Immune Profiling Panel. We analyzed RNA isolated from the right lateral half of tongues of mice 1, 2, 4, and 7 wk after transplant of $MOC1^{Cas9}$ or $MOC1^{AhR\text{-}KO}$ cells and identified 82, 206, 377, and 516 significantly differentially expressed genes at those timepoints, respectively ($P < 0.05$) (Fig. 1*D*).

Consistent with the rapid clearance of $MOC1^{AhR\text{-}KO}$ but not $MOC1^{Cas9}$ tumors, NanoString data revealed significantly higher expression of gene modules defining cytotoxic T lymphocytes (CTLs) in $MOC1^{AhR\text{-}KO}$ tumors as compared with tissue from naïve mice or from the control tumor at the 1-wk timepoint (Fig. 1 *E*, *Top*). By 2 wk, when $MOC1^{AhR\text{-}KO}$ tumors were cleared, the CTL signal in $MOC1^{AhR\text{-}KO}$-injected tongue was no longer significantly different from either the naïve or the Cas9 controls (Fig. 1 *E*, *Bottom*). While expression of the CTL module tended to be higher in control $MOC1^{Cas9}$ tumors than in naïve tissue at both timepoints, it did not reach statistical significance ($P = 0.051$).

Ingenuity Pathway Analysis (IPA) of the differentially expressed genes revealed that, 1 wk after injection, transcriptional modules associated with increased T cell responsiveness, including Th1 and Th2 pathway activation, CD28, iCOS-iCOSL, NF-κB activation, interferon, TREM1, and IL-6 signaling pathways, were significantly higher in $MOC1^{AhR\text{-}KO}$-transplanted tongues than $MOC1^{Cas9}$-transplanted tongues (Fig. 1*F* and *SI Appendix*, Table S1). Notably, IL-6 is a biomarker of OSCC progression (38) and NF-κB and IL-6 have both been reported to be regulated by the AhR in various contexts (8, 28, 39). The inverse pattern was seen by 2 wk, when tumors became undetectable in the $MOC1^{AhR\text{-}KO}$-injected tongues. Notably, concomitant with clearance of the $MOC1^{AhR\text{-}KO}$ tumor by 2 wk and through 7 wk, transcriptional modules associated with T cell exhaustion were significantly lower in tongues from $MOC1^{AhR\text{-}KO}$-injected mice than in controls.

These data indicate the successful clearance of the $MOC1^{AhR\text{-}KO}$ tumor by the immune system by 2 wk and an ongoing but insufficient/exhausted immune response to the $MOC1^{Cas9}$ tumor throughout the experimental period.

Control $MOC1^{Cas9}$ but Not $MOC1^{AhR\text{-}KO}$ Cells Induce Multiple Immune Checkpoint Markers. We next hypothesized that the transcriptional changes associated with immune modulation in the tongues of $MOC1^{AhR\text{-}KO}$-implanted mice (Fig. 1) would be reflected in the distribution of immune cells expressing markers of T cell exhaustion and immune checkpoint mediators in the submandibular and cervical tumor-draining lymph nodes (tdLNs). Analysis of the submandibular tdLNs in humans is prognostic of HNSCC outcomes and a surrogate for tumor-mediated immunosuppression (40, 41). Note that this flow cytometry analysis could not be performed within the tumor itself, since an insufficient number of leukocytes can be recovered from this highly muscular organ for flow cytometric analysis of multiple cell subsets.

While the percentage of $CD4^+$ and $CD8^+$ cells was similarly reduced in tdLNs of both the $MOC1^{Cas9}$- and $MOC1^{AhR\text{-}KO}$-implanted mice at 1 wk compared to naïve mice (Fig. 2*A*), the absolute number of $CD4^+$ and $CD8^+$ cells was significantly higher ($P < 0.05$) in the tdLNs from the $MOC1^{AhR\text{-}KO}$-implanted mice compared to $MOC1^{Cas9}$-implanted mice and naïve mice (Fig. 2*B*), a result consistent with a rapid and effective immune response to the $MOC1^{AhR\text{-}KO}$ cells. The number and percentage of $CD4^+$ and $CD8^+$ T cells in tdLNs from $MOC1^{AhR\text{-}KO}$-injected mice returned to baseline levels at 2 wk, when tumors had been cleared, while the number of $CD4^+$ and $CD8^+$ T cell subsets in the tdLNs from $MOC1^{Cas9}$-injected mice increased over time (Fig. 2 *A* and *B*).

Further, the percentage and absolute number of $CD4^+$ $IFN\gamma^+$ T cells spiked at 1 wk ($P < 0.0001$) and then returned to baseline at 2 wk in the tdLNs from $MOC1^{AhR\text{-}KO}$-transplanted mice while the percentage and absolute number of $CD4^+$ $IFN\gamma^+$ T cells from the tdLNs of $MOC1^{Cas9}$-transplanted mice slowly rose over the first 4 wk of the experiment (Fig. 2 *C* and *E*).

With regard to immune checkpoint/exhaustion markers on T cells, there was a significant increase in the percentage of $Lag3^+$, $CTLA4^+$, and $CD39^+CD4^+$ T cells at 1 to 2 wk in the tdLNs from $MOC1^{AhR\text{-}KO}$-injected mice (Fig. 2*D*). These increases were reflected in significant increases in the absolute number of these cells at 1 to 2 wk (Fig. 2*F*). The absolute number of $PD1^+CD4^+$ T cells also spiked at 1 wk in $MOC1^{AhR\text{-}KO}$-injected mice while their

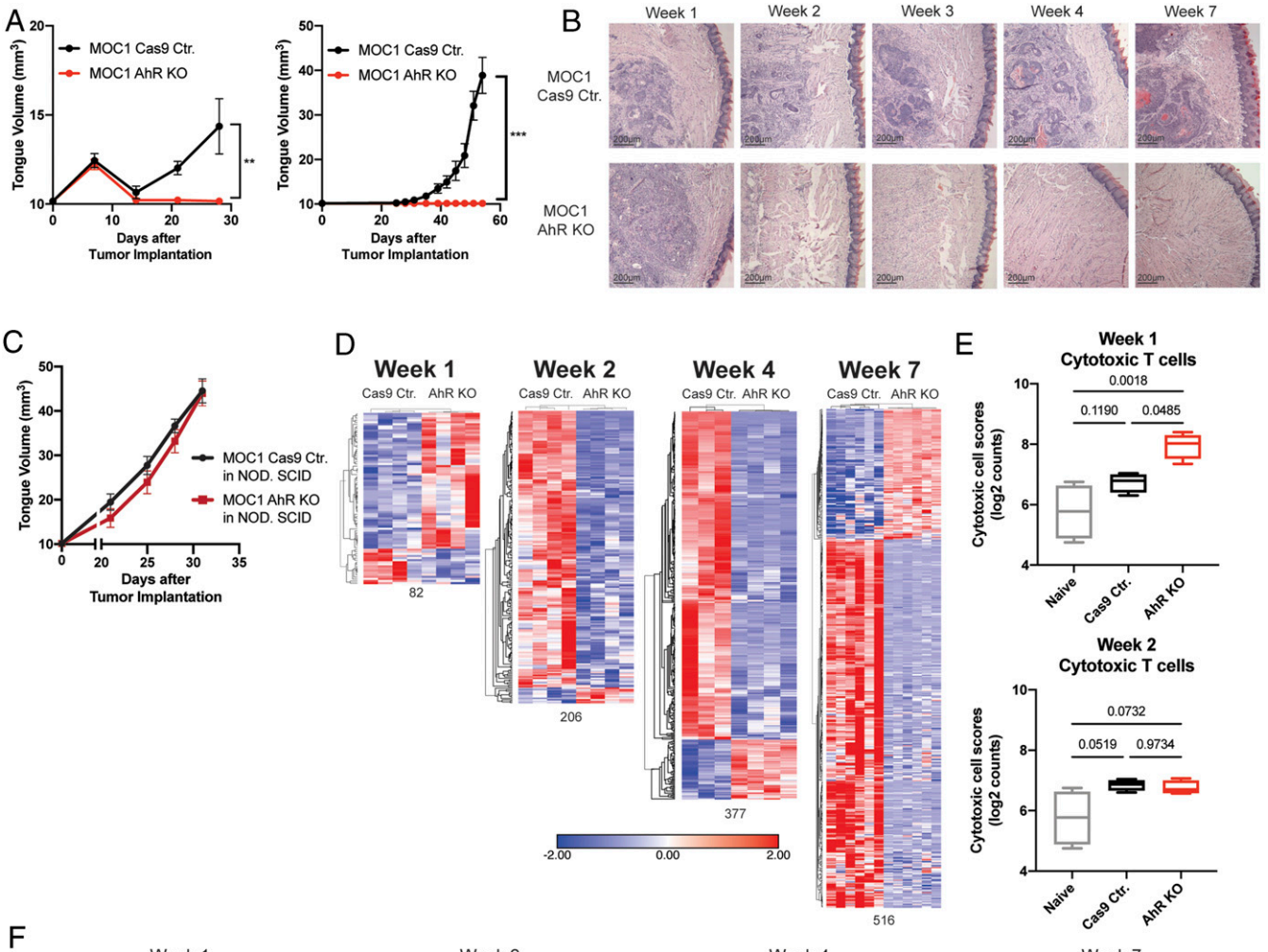

Fig. 1. AhR knockout in MOC1 cells prevents orthotopic tumor growth. Control MOC1^{Cas9} or MOC1$^{AhR\text{-}KO}$ (3×10^5) cells were injected into the right lateral side of the tongue ~1.5 mm from the tip of the tongue of C57BL/6 or NOD/SCID mice using a 27 1/2 gauge needle so that a bulbous mass formed in the center of the tongue. Tumor size was determined with a caliper. For histological analyses or mRNA extraction, entire tongues were removed and bisected down the middle from tip to back. In instances where histology was performed, the right half of the tongue was used for RNA isolation and the left half for histology; otherwise the entire tongue was used for RNA isolation. (*A*) Tongue volumes were measured once/week for 28 d (*Left*) or twice/week for 7 wk (*Right*) after injection. Small white tumors were visible 1 wk after injection of MOC1^{Cas9} or MOC1$^{AhR\text{-}KO}$ cells. Data are means ± SEM, representative of one experiment (*Left*) or more than three independent experiments (*Right*), $n = 4$ to 8 mice per group. *P* values are derived using two-way ANOVA,$^{**}P < 0.01$ and $^{****}P < 0.0001$. (*B*) Representative H&E staining of tongue tissue from mice injected 1, 2, 3, 4, or 7 wk prior with MOC1^{Cas9} cells or MOC1$^{AhR\text{-}KO}$ cells. (*C*) Tongue volume in immunodeficient NOD/SCID mice injected orthotopically with 3×10^5 MOC1$^{AhR\text{-}KO}$ cells or MOC1^{Cas9} control cells. Data are means ± SEM, $n = 6$ mice per group. (*D–F*) Gene expression analysis using the NanoString PanCancer Immune Profiling Panel on mRNA isolated from the right half of tongues from MOC1^{Cas9} cell-injected mice compared to MOC1$^{AhR\text{-}KO}$-injected mice at various timepoints after tumor injection, $n = 3$ to 6 mice per group. (*D*) Heat map of differentially regulated genes at 1, 2, 4, or 7 wk postinjection with a $P < 0.05$. Data are $\log_2$ transformed, row centered, and saturated at −2 and +2 for visualization. (*E*) Cytotoxic T cell profiling scores based on the gene expression profiles of naïve mice, MOC1$^{AhR\text{-}KO}$-injected mice, or MOC1^{Cas9}-injected mice. *P* values were derived using a one-way ANOVA and Tukey's multiple comparisons test. (*F*) IPA of the differentially regulated genes in MOC1$^{AhR\text{-}KO}$-injected tongues compared to MOC1^{Cas9}-injected tongues at 1, 2, 4, or 7 wk postinjection. Pathways associated with positive z-scores are in orange; pathways associated with negative z-scores are in blue; the relative strength of the z-score is represented by the intensity of the color.

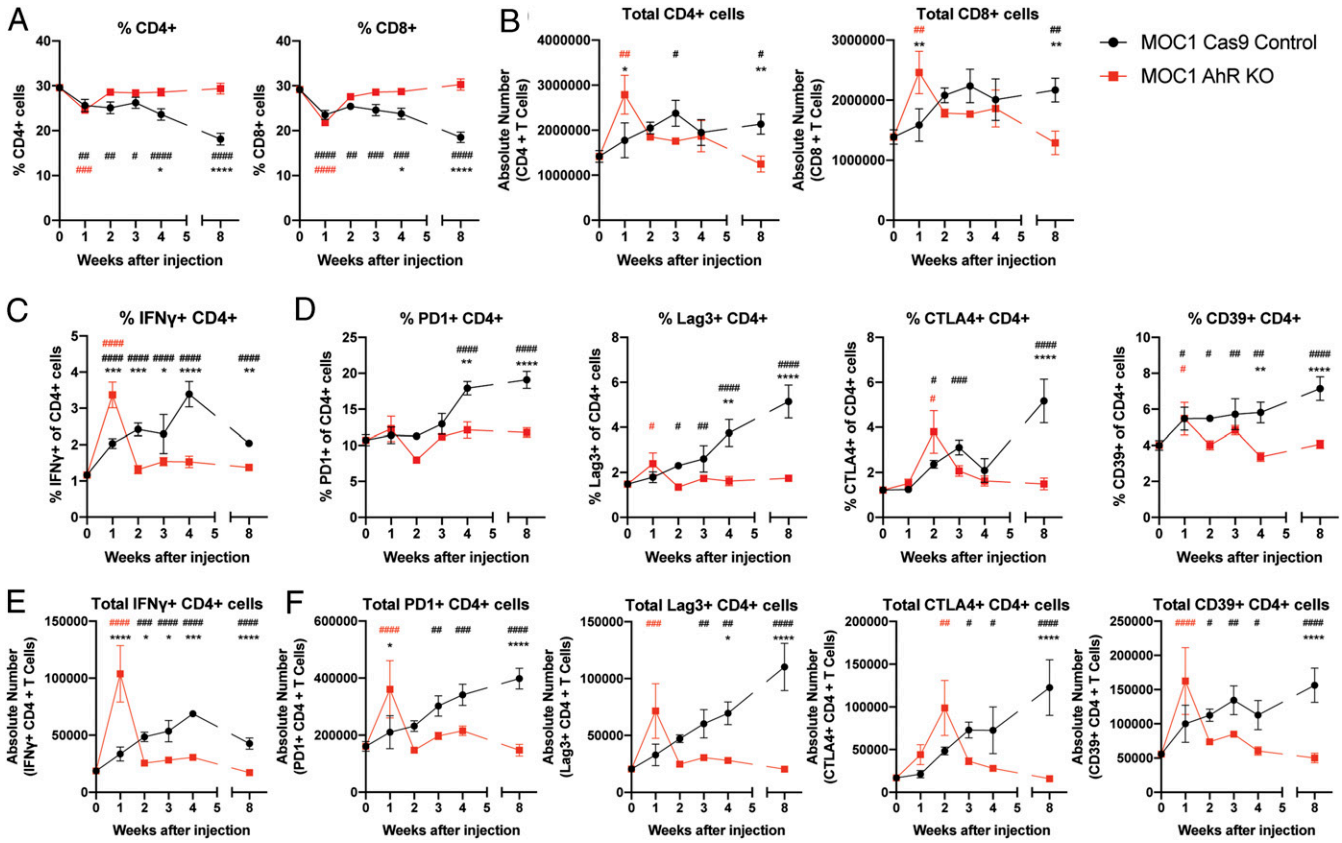

Fig. 2. AhR knockout in MOC1 cells alters the phenotype of T cells in tdLNs. Mice were injected orthotopically with $MOC1^{Cas9}$ or AhR^{KO} MOC1 cells as in Fig. 1. tdLNs were harvested from mice injected 1, 2, 3, 4, or 8 wk prior with tumor or from naïve mice (shown as 0-wk timepoint) and analyzed by flow cytometry for the percentage and absolute number of (*A* and *B*) $CD4^+$ and $CD8^+$ T cells; (*C* and *E*) $IFN\gamma^+$ $CD4^+$ T cells; and (*D* and *F*) $PD1^+$, $Lag3^+$, $CTLA4^+$, and $CD39^+$ CD4 T cells. Data are means ± SEM, $n = 4$ to 6 mice per group. *P* values are derived using two-way ANOVA and Sidak's multiple comparisons test. Black hashtags represent a significant difference between $MOC1^{Cas9}$-injected mice and naïve mice; red hashtags represent a significant difference between $MOC1^{AhR\text{-}KO}$-injected mice and naïve mice; and black stars represent a significant difference between $MOC1^{Cas9}$-injected mice and $MOC1^{AhR\text{-}KO}$-injected mice. $^{*,\#,\#}P < 0.05$; $^{**,\#\#,\#\#}P < 0.01$; $^{***,\#\#\#,\#\#\#}P < 0.001$; $^{****,\#\#\#\#,\#\#\#\#}P < 0.0001$.

percentage and numbers returned to baseline after an initial spike. In contrast, the percentage and absolute number of $CD4^+$ T cells expressing PD1, Lag3, CTLA4, and CD39 steadily increased after injection of $MOC1^{Cas9}$ control cells (Fig. 2 *D* and *F*).

With regard to non-T cells, injection of either $MOC1^{Cas9}$ or $MOC1^{AhR\text{-}KO}$ cells tended to increase the percentage and number of $PD\text{-}L1^+$ granulocytic-myeloid-derived suppressor cells (G-MDSC; defined as $CD45^+CD11b^+Ly6c^-Ly6g^{high}$) and dendritic cells (DCs, defined as $CD45^+CD11c^+$), as well as $CD39^+$ G-MDSC cells and macrophages (defined as $CD45^+CD11b^+Ly6g^-Ly6c^+$) in the tdLNs 1 wk after tumor cell transplantation (Fig. 3 *A*, *B*, *D*, and *E*). The percentage and numbers of these cell subsets decreased essentially to baseline levels in the tdLNs of mice transplanted with $MOC1^{AhR\text{-}KO}$ cells by 2 wk, while they increased gradually in the tdLNs of mice transplanted with $MOC1^{Cas9}$ cells (Fig. 4 *A*, *B*, *D*, and *E*).

We also observed a significant increase in the percentage and number of $CCR2^+$ macrophages in $MOC1^{Cas9}$-transplanted mice at the 8-wk timepoint (Fig. 3 *C* and *F*), suggesting an increased ability of macrophages to migrate to the tumor.

We then returned to the NanoString data to determine if the same changes in immune checkpoint/exhaustion markers could be observed on the mRNA level in tongues as was seen by flow cytometry within tdLNs. Indeed, a similar profile of *Pdcd1* (PD-1), *Lag3*, *Ctla4*, *Cd274* (PD-L1), and *Ifnγ* mRNA levels was observed. Thus, all five genes from $MOC1^{AhR\text{-}KO}$-injected tongues tended to increase at 1 wk (although only *Cd274* was statistically significant) and to return to baseline at 2 wk, while all five genes increased over time in the $MOC1^{Cas9}$-injected tongues (Fig. 3*G*). Interestingly, we also observed a steady increase in mRNA expression of the *Ccl2* chemokine in the tongues from $MOC1^{Cas9}$-injected mice (Fig. 3*H*), a result that parallels the increase in $CCR2^+$ macrophages in tdLNs of $MOC1^{Cas9}$ but not $MOC1^{AhR\text{-}KO}$-injected mice and is consistent with recruitment of potentially immunosuppressive $CCR2^+$ macrophages by its ligand (CCL2) to the tumor, as in glioblastoma (13). CCL2 production and tumor infiltration of $CCR2^+$ macrophages has been linked to poor outcomes in OSCC (42–44).

AhR Knockout Induces a Long-Lasting, Systemic, Antitumor Immune Response. Given the immune profile observed in recipients of $MOC1^{AhR\text{-}KO}$ cells, we hypothesized that mice previously exposed to $MOC1^{AhR\text{-}KO}$ tumors would have significant immunologic memory for the neoantigens expressed in $MOC1^{WT}$ cells. To test this hypothesis, we challenged C57BL/6J mice with 3×10^5 $MOC1^{WT}$ cells 100 d after a previous orthotopic injection of 3×10^5 $MOC1^{AhR\text{-}KO}$ cells.

As expected, $MOC1^{AhR\text{-}KO}$ cells injected orthotopically failed to generate tumors after 2 wk (Fig. 4 *A*, *Left*, red line). Remarkably, $MOC1^{AhR\text{-}KO}$-injected mice challenged orthotopically 100 d later with $MOC1^{WT}$ cells also failed to generate wild-type tumors (Fig. 4 *A*, *Right*, red line), suggesting a long-term memory response. Immunophenotyping of submandibular and cervical LNs 70 d after the secondary challenge with MOC^{WT} cells in mice previously "immunized" with $MOC1^{AhR\text{-}KO}$ cells showed increased percentages of

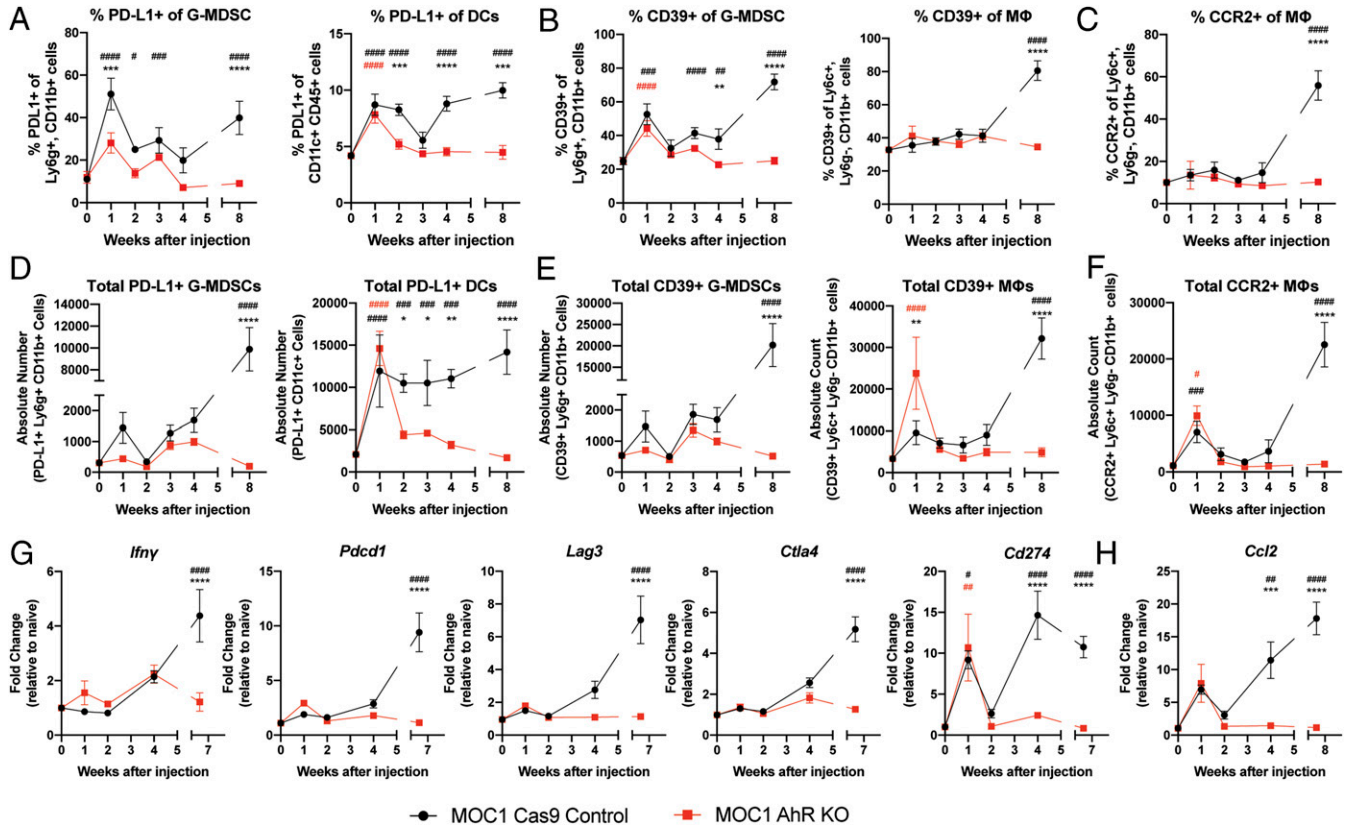

Fig. 3. AhR knockout in MOC1 cells alters the phenotype of myeloid cells in tdLNs. Mice were injected orthotopically with either $MOC1^{Cas9}$ or $MOC1^{AhR\text{-}KO}$ cells as in Fig. 1. tdLNs were harvested from mice injected 1, 2, 3, 4, or 8 wk prior with tumor or from naïve mice (shown as 0-wk timepoint) and analyzed by flow cytometry for the percentage and absolute number of (*A* and *D*) PD-L1$^+$ G-MDSCs and DCs; (*B* and *E*) CD39$^+$ G-MDSCs and macrophages (MΦ); and (*C* and *F*) CCR2$^+$ macrophages (MΦ). (*G* and *H*) *Ifnγ*, *Pdcd1*, *Lag3*, *Ctla4*, *Cd274*, and *Ccl2* mRNA expression in the tongue of mice injected 1, 2, 3, 4, or 8 wk previously as measured by NanoString, and normalized to expression in tongues from naïve mice, as in Fig. 1 *D*–*F*. Data are means ± SEM, $n = 4$ to 6 mice per group. *P* values are derived using two-way ANOVA and Sidak's multiple comparisons test. Black hashtags represent a significant difference between $MOC1^{Cas9}$-injected mice and naïve mice; red hashtags represent a significant difference between $MOC1^{AhR\text{-}KO}$-injected mice and naïve mice; and black stars represent a significant difference between $MOC1^{Cas9}$-injected mice and $MOC1^{AhR\text{-}KO}$-injected mice.*,#,#$P < 0.05$; **,##,##$P < 0.01$; ***,###,###$P < 0.001$; ****,####,####$P < 0.0001$.

$CD4^+$ and $CD8^+$ T cells and decreased representation of PD-1^+, $Lag3^+$, and $CD39^+$ $CD4^+$ T cells as compared with naïve mice injected with wild-type $MOC1^{WT}$ cells (Fig. 4*B*). While no tumors were detected at 70 d, tongues from $MOC1^{AhR\text{-}KO}$ immunized mice were not "normal" in that NanoString analysis of tongue mRNA showed: 1) a different transcriptomic profile and an increase in T cells in general and cytotoxic cells in particular relative to tongues from naïve mice, and 2) an increase in multiple markers of T cell signaling activity, including Th1, Th2, OX40, Erk5, PKCΦ, and NF-κB signaling pathways (*SI Appendix*, Fig. S2).

Nearly the same results were seen with another immunogenic OSCC cell line, MOC22 (33, 34). That is, $MOC22^{Cas9}$ control but not $MOC22^{AhR\text{-}KO}$ cells injected orthotopically generated a significant tumor burden (*SI Appendix*, Fig. S3, *Left*). $MOC22^{AhR\text{-}KO}$-injected mice challenged orthotopically 150 d later with $MOC22^{WT}$ cells generated small tumors that failed to grow until at least day 70 (*SI Appendix*, Fig. S3, *Right*), again suggesting a long-term antitumor immunity.

To determine if the tumor-specific immunity could also be induced systemically, we injected mice subcutaneously with $MOC1^{AhR\text{-}KO}$ cells 2 wk prior to, or on the same day as, orthotopic challenge with $MOC1^{WT}$ cells. Subcutaneous tumors were never observed in $MOC1^{AhR\text{-}KO}$-injected mice. Subcutaneous injection of $MOC1^{AhR\text{-}KO}$ cells 2 wk prior to orthotopic $MOC1^{WT}$ challenge completely protected mice from wild-type tumor growth (Fig. 4*C*, red lines). However, subcutaneous $MOC1^{AhR\text{-}KO}$ cell transplant the same day as orthotopic challenge with $MOC1^{WT}$ cells did not protect mice from $MOC1^{WT}$ tumor growth (Fig. 4 *C*, *Middle*, black line). Correlating with our previous observations, we documented a higher percentage of $CD4^+$ and $CD8^+$ T cells (Fig. 4*D*) and a lower percentage of PD-1^+, $Lag3^+$, $CTLA4^+$, and $CD39^+$ $CD4^+$ T cells (Fig. 4*E*) in the LNs of mice initially injected subcutaneously with $MOC1^{AhR\text{-}KO}$ cells, then challenged with $MOC1^{WT}$ cells orthotopically 2 wk later and sacrificed 60 d after the $MOC1^{WT}$ challenge. The percentage of PD-$L1^+$ G-MDSCs and DCs, and $CD39^+$ G-MDSCs, was lower in LNs from $MOC1^{AhR\text{-}KO}$ immunized, $MOC1^{WT}$-challenged mice (Fig. 4 *F* and *G*). As with the primary challenge (Fig. 3 *C* and *F*), the percentage of $CCR2^+$ macrophages was significantly lower in LNs from $MOC1^{AhR\text{-}KO}$-immunized and $MOC1^{WT}$-challenged mice (Fig. 4*H*).

Finally, when $MOC22^{WT}$ cells were used as the secondary challenge, tumors grew approximately as well in naïve mice as in mice previously transplanted with $MOC1^{AhR\text{-}KO}$ cells (*SI Appendix*, Fig. S4), indicating that immunity induced in $MOC1^{AhR\text{-}KO}$-injected mice is predominantly tumor specific. These results indicate that the potent immunity induced by $MOC1^{AhR\text{-}KO}$ cells is long lasting, systemic, tumor-specific, and takes no more than 2 wk to induce.

The AhR Modulates Immune Signaling in MOC1 Tumor Cells. To elucidate some of the AhR-dependent mechanisms that may be regulating tumor immunity, we compared the transcriptional profiles of control $MOC1^{Cas9}$ and $MOC1^{AhR\text{-}KO}$ MOC1 cells. We identified 245 significantly differentially expressed genes (Fig. 5 *A* and *B*; $P < 0.05$), including 180 genes that were down-regulated

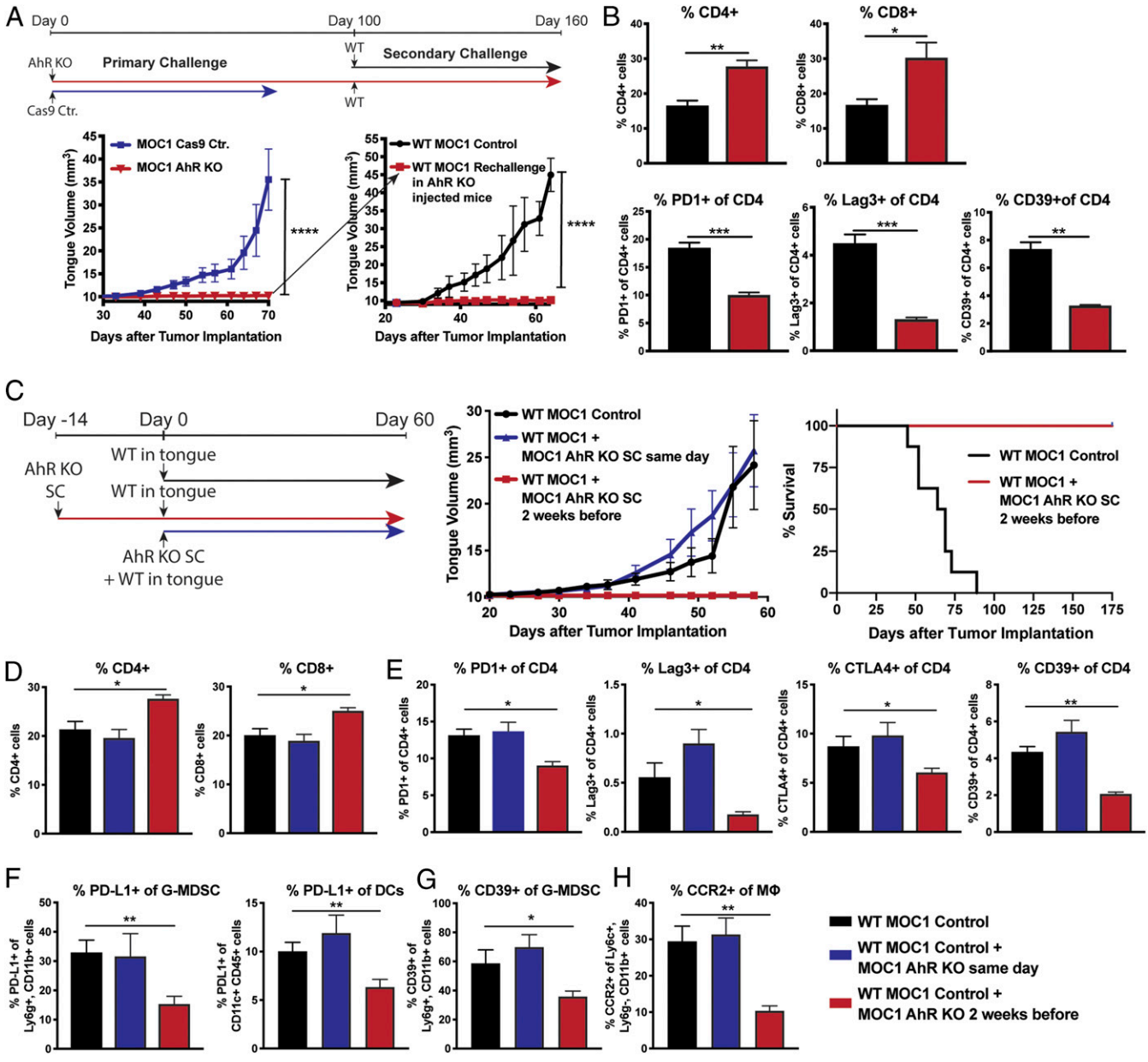

Fig. 4. AhR knockout in MOC1 cells induces tumor-specific immunity. (*A*, *Top*) Timeline. (*A*, *Bottom Left*) Tongue volume after orthotopic injection of 3×10^5 $MOC1^{Cas9}$ or $MOC1^{AhR\text{-}KO}$ cells. (*A*, *Bottom Right*) One hundred days after initial injection with $MOC1^{AhR\text{-}KO}$ cells mice were rechallenged orthotopically with 3×10^5 $MOC1^{WT}$ cells. As a control, naïve mice were injected into the tongue with $MOC1^{WT}$ cells. Tumor volume was measured after $MOC1^{WT}$ cell injection. Data are means ± SEM, representative of two independent experiments, $n = 6$ mice per group. ***$P < 0.0001$ (two-way ANOVA). (*B*) TdLNs were analyzed at day 65 post-$MOC1^{WT}$ injection for the percentage of $CD4^+$ and $CD8^+$ T cells and $PD1^+$, $Lag3^+$, and $CD39^+$ CD4 T cells. Data are means + SEM, representative of two independent experiments, $n = 6$ mice per group. *$P < 0.05$, **$P < 0.01$, ***$P < 0.001$ (Student's *t* test). (*C*, *Left*) Timeline. (*C*, *Middle*) Tongue volumes in mice injected subcutaneously on the right and left flanks with 3×10^5 $MOC1^{AhR\text{-}KO}$ cells either the same day (blue line) or 2 wk previously (red line) and then challenged with $MOC1^{WT}$ cells injected orthotopically. Tongue tumor size was tracked after $MOC1^{WT}$ transplant. As a positive control, $MOC1^{WT}$ cells were injected orthotopically into naïve mice (black line). (*C*, *Right*) Survival curve for an independent repeat of the experiment shown in Fig. 5 *C*, *Middle* with mice injected 2 wk prior to $MOC1^{WT}$ challenge with $MOC1^{AhR\text{-}KO}$ cells. Data are means ± SEM, $n = 8$ mice per group. At day 58 post-$MOC1^{WT}$ cell injection, tdLNs were analyzed for percentage of $CD4^+$ and $CD8^+$ T cells (*D*), $PD1^+$, $Lag3^+$, $CTLA4^+$, and $CD39^+$ CD4 T cells (*E*), PD-$L1^+$ G-MDSCs and DCs (*F*), $CD39^+$ G-MDSCs (*G*), and $CCR2^+$ macrophages (MΦ) (*H*). For *D*–*H*, data are means + SEM, $n = 6$ mice per group. *$P < 0.05$, **$P < 0.01$ (one-way ANOVA).

and 65 genes that were up-regulated in $MOC1^{AhR\text{-}KO}$ cells as compared with $MOC1^{Cas9}$ controls. Ingenuity Pathway Analysis of the differentially expressed genes revealed that AhR knockout down-regulated pro-tumorigenic inflammatory signaling pathways, including IL-1, IL-6, IL-8, STAT3, NF-κB, and iNOS (Fig. 5*C*). Conversely, several pathways associated with tumor suppressor function, including PPAR and PTEN (45, 46), were significantly higher. Correlating with our in vivo gene-profiling results obtained from the tumor microenvironment (Fig. 1 *D*–*F*) and immune phenotyping data from tdLNs (Figs. 2–4), the T cell exhaustion signaling pathway was significantly lower in $MOC1^{AhR\text{-}KO}$ cells than in $MOC1^{Cas9}$ cells (Fig. 5*C*). With regard to specific genes, AhR knockout significantly down-regulated genes encoding PD-L1 (*Cd274*) (Fig. 5*D*) and the chemokines CXCL2, CXCL3, and CXCL5 (Fig. 5*B*, red circles and Fig. 5*D*) known to promote the recruitment and generation of MDSCs (45, 47).

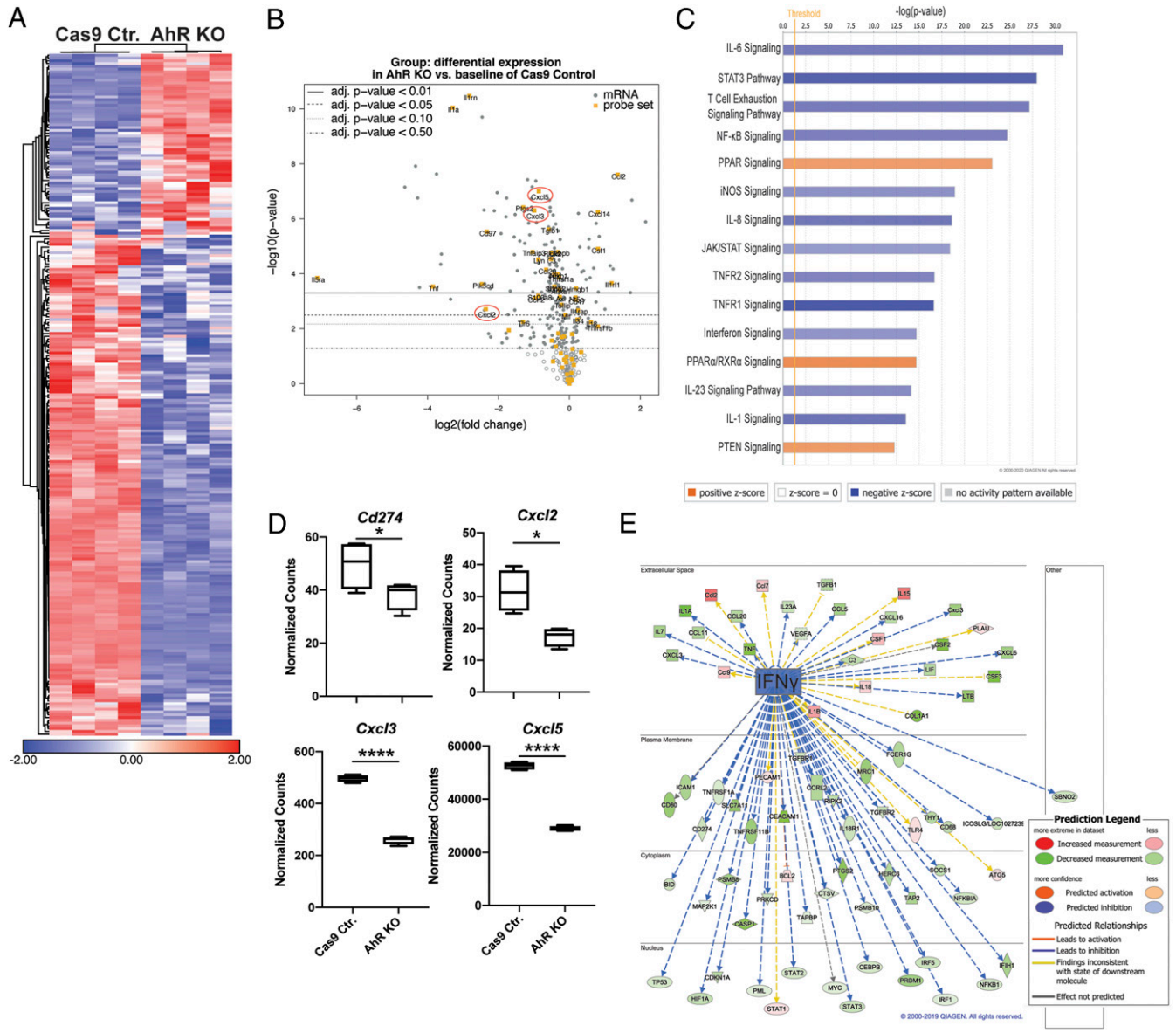

Fig. 5. The AhR modulates immune signaling pathways in MOC1 tumor cells. Gene expression analysis using the NanoString PanCancer Immune Profiling Panel on mRNA isolated from MOC1^{Cas9} compared with MOC1$^{AhR\text{-}KO}$ cells in vitro. $n = 4$ biological replicates/group. (*A*) Heat map of differentially regulated genes with a $P < 0.05$. Data are $\log_2$ transformed, row centered, and saturated at −2 and +2 for visualization. (*B*) Volcano plot of differential gene expression. Yellow squares represent genes belonging to the inflammatory gene set identified by NanoString. Red circles highlight chemokines CXCL2,3,5 involved in tumor inflammation. (*C*) IPA of the differentially regulated genes in MOC1$^{AhR\text{-}KO}$ cells compared to MOC1^{Cas9} cells. (*D*) mRNA expression of *Cd274*, *Cxcl2*, *Cxcl3*, and *Cxcl5* in MOC1^{Cas9} cells and MOC1$^{AhR\text{-}KO}$ cells. Data are means + SEM, $n = 4$ biological replicates/group. *$P < 0.05$ and ****$P < 0.0001$ (Student's *t* test). (*E*) IPA of the IFNγ signaling pathway in MOC1$^{AhR\text{-}KO}$ cells.

Finally, AhR knockout reduced expression of numerous components within the IFNγ signaling pathway ($P = 2.65E^{-59}$, Fig. 5*E*), suggesting that AhR signaling may regulate the response of MOC1 cells to IFNγ produced by nonmalignant cells, e.g., IFNγ$^+$ T cells that expand over time in the tdLNs of MOC1^{Cas9}-transplanted mice (Fig. 2 *D* and *F*) and coincident with the accumulation of *Ifnγ* in the tongue TME (Fig. 3*G*). These results appear to reflect multiple mechanisms through which the AhR may moderate tumor immunity and suggest that chronic IFNγ signaling drives protumorigenic responses in these OSCC cells.

The AhR Transcriptionally Regulates *Cd274*/PD-L1. The NanoString data showing a significant decrease in MOC1 *Cd274* after AhR deletion (Fig. 5*D*) suggest that the AhR may directly or indirectly regulate PD-L1 expression on malignant cells and thereby contribute to expression of T cell exhaustion markers in the tumor injection site (Fig. 1) and in the tdLNs (Figs. 2 and 3). To confirm that the AhR regulates *Cd274*/PD-L1 in MOC1 cells, *Cd274* mRNA was quantified in MOC1^{Cas9} or MOC1$^{AhR\text{-}KO}$ cells in the presence or absence of vehicle (dimethylsulfoxide/DMSO) or the prototypic environmental AhR agonist, 2,3,7,8-tetrachlorodibenzo-p-dioxin (TCDD) (1 nM) by qPCR. AhR knockout significantly reduced and TCDD significantly increased (Fig. 6 *A*, *Left* and *Middle*) *Cd274* levels. The failure of TCDD to increase *Cd274* in MOC1$^{AhR\text{-}KO}$ cells (Fig. 6 *A*, *Right*) indicates that the *Cd274* induction with this potent AhR ligand is indeed AhR dependent. Similarly, AhR knockout decreased and TCDD increased the percentage of PD-L1$^+$ MOC1 cells as measured by flow cytometry (Fig. 6 *B*, *Left* two graphs). This increase

in the percentage of PD-L1$^+$ cells reflects a change in the amount of PD-L1 on a per cell basis, as indicated by lower mean fluorescence intensities (MFIs) in MOC1$^{AhR\text{-}KO}$ cells or in control cells after TCDD treatment (Fig. 6 *B*, *Right* two graphs). That these AhR-dependent PD-L1 effects occurred at a transcriptional level was supported by a significant ($P < 0.001$) increase in PD-L1 reporter activity after treatment with the AhR agonists kynurenine or TCDD (Fig. 6*C*).

Analysis of the *Cd274* promoter sequence revealed five potential consensus AhR response elements (AhREs) within a 1,943-bp region extending from -1,723 to +220 bp (beginning at nucleotides -1,555, -1,546, -374, +32, and +43). Deletion of a 680-bp region from -460 to +220 removing AhREs beginning at -374, +32, and +43, or a double deletion removing AhREs -1,555, -1,546, +32, and +43 but preserves AhRE -374 in a *Cd274* reporter plasmid, completely ablated baseline reporter activity (Fig. 6*D*). Preservation of the -132 to +220 fragment containing AhREs +32 and +43 was sufficient for maximal reporter activity.

Site-specific mutations were then generated to determine if the critical sequences in the -132 to +220 fragment of the *Cd274* promoter were functional AhREs. Mutation of either predicted AhRE +32 or +43 significantly suppressed promoter activity and mutation of both sites almost completely eliminated reporter activity (Fig. 6*E*). These results are consistent with the hypothesis that the AhR regulates *Cd274* expression through direct transactivation of its promoter.

IFNγ Regulates *Cd274* and *Ido* through the AhR. NanoString data (Fig. 5*E*) suggest that MOC1 OSCC cells may be responsive to IFNγ signaling and data from Figs. 1, 2*E*, and 3*G* indicate that IFNγ is likely to be present in the TME. As expected, qPCR analysis of mRNA from tongues injected 8 wk previously with MOC1^{Cas9} or MOC1$^{AhR\text{-}KO}$ cells indicated ~140-fold higher levels of *Ifnγ* in the former as compared with the latter (Fig. 7*A*). Since IFNγ induces PD-L1 expression on tumor and immune cells (46, 48), we evaluated the effect of exogenous IFNγ, in the context of AhR signaling, on PD-L1 expression by malignant cells in vitro.

Consistent with the NanoString (Fig. 5*D*) and previous qPCR (Fig. 6*A*) data, AhR knockout significantly reduced baseline *Cd274* expression in MOC1 cells as quantified by qPCR (Fig. 7*B*, first two bars). Consistent with previous studies (49), IFNγ increased *Cd274* expression in MOC1^{Cas9} control cells (Fig. 7*B*). However, this *Cd274* induction was significantly lower in MOC1$^{AhR\text{-}KO}$ cells, indicating that IFNγ induction of *Cd274* in MOC1 cells is at least partially AhR dependent.

While these studies indicate that the AhR contributes to PD-L1 expression in malignant cells, they do not explain how AhR deletion in malignant cells decreases the percentage of PD-L1$^+$ G-MDSCs and DCs in the tdLNs of MOC1$^{AhR\text{-}KO}$-injected mice. One possibility is through AhR control of IDO, the resulting production of AhR ligand(s) by malignant cells, and the activation of the AhR in immune cells. This AhR-mediated enhancement of IDO would not preclude involvement of IFNγ, which also induces IDO (49, 50). To assess these nonmutually exclusive possibilities, *Ido1*, *Ido2*, *and Tdo2* were quantified in MOC1^{Cas9} and MOC1$^{AhR\text{-}KO}$ MOC1 cells in vitro by qPCR. Significant baseline levels of both *Ido1* and *Ido2* (Fig. 7 *C*, *Left* and *Right* first bars), but not *Tdo2*, were detected in control cells. In contrast, relatively little *Ido1* or *Ido2* was detected in MOC1$^{AhR\text{-}KO}$ cells (Fig. 7*C*, second bars). IFNγ dramatically increased *Ido1* and *Ido2* levels. Remarkably, IFNγ-mediated induction of these genes was >70% lower in MOC1$^{AhR\text{-}KO}$ cells than MOC1^{Cas9} cells, demonstrating that, like IFNγ induction of *Cd274* (Fig. 7*B*), IFNγ up-regulation of *Ido1/2* is AhR regulated. Further, as could be predicted from these data, *Ido1/2* levels in tongue tissue from MOC1$^{AhR\text{-}KO}$-injected mice were significantly lower than in MOC1^{Cas9} tumors (Fig. 7*D*).

These data imply a role for the AhR in the direct transcriptional control of *Cd274* and IFNγ induction of *Cd274*, *Ido1*, and *Ido2*. Further, chronic IFNγ production in the tumor microenvironment, as opposed to transient early IFNγ production as in the IFNγ spike seen 1 wk after MOC1$^{AhR\text{-}KO}$ cell injection (Fig. 2*C*), may contribute to the stoking of a IFNγ→AhR→IDO→AhR ligand amplification loop in malignant cells and suppression of immune cells in the TME through AhR ligand production and AhR-dependent PD-L1 induction. Thus, this study directly links the AhR to control of IFNγ induction of critical immune checkpoints, i.e., PD-L1 and IDO.

Discussion

The AhR has been implicated in the pathogenesis of several cancer subtypes including HNSCC (6–16). While chronically active AhR within malignant cells has been linked to cancer aggressiveness (6, 7, 17, 18), AhR within immune cells has been linked to immunosuppression (21, 22, 24, 27, 28, 51, 52). Here, we tested the hypothesis that the AhR, chronically active within malignant cells, also has an impact on immune cells in the TME.

While MOC1$^{AhR\text{-}KO}$ cells grew at the same rate as MOC1^{Cas9} control cells in immunodeficient mice, they failed to grow for more than 1 wk in immunocompetent mice (Fig. 1 *A*–*C*). This complete rejection of MOC1$^{AhR\text{-}KO}$ cells was characterized by a spike in T cell signaling in the tumor and CD4$^+$ and CD8$^+$ T cells in the tdLNs and was followed by a decrease in the number and percentage of CD4$^+$ T cells expressing PD-1, Lag3, CTLA4, and CD39; G-MDSCs and DCs expressing PD-L1 and CD39; and MΦs expressing CD39 and CCR2. This immune profile correlated with reduced PD-L1 and Ido expression in malignant cells and the induction of long-lasting, systemic, and tumor antigen-specific immunity leading to the conclusion that malignant cell AhR alters TME conditions to favor immunosuppression.

One mechanism through which malignant cell AhR may affect immunosuppression is through PD-L1 up-regulation (Fig. 6). AhR control of *Cd274*/PD-L1expression in MOC1 cells is reminiscent of a previous study demonstrating that tobacco carcinogen-induced AhR activation induces PD-L1 on normal lung epithelial cells (35). The significance of AhR control of PD-L1 is underscored by the finding that PD-1/PD-L1 blockade is most effective in lung cancer when malignant cells express high AhR levels (35). A second mechanism of immunosuppression may be through malignant cell production of excess kynurenine enforced by the AhR→IDO→AhR ligand loop (enhanced by IFNγ) and kynurenine's effect on TME immune cells. As in malignant cells, kynurenine may enhance PD-L1 expression on G-MDSC, macrophages, and DCs, all of which express AhR (28, 53, 54). AhR activation, in some cases by kynurenine, also induces the immunosuppressive CD39 ectoenzyme on macrophages and T cells through direct transcriptional control (13, 23, 55, 56). Furthermore, PD-1 expression on CD8$^+$ T cells in the TME has been linked to the AhR and "transcellular" Kyn produced by melanomas (31). Consistent with these possibilities is the increase in the T cell exhaustion module in the tongues of MOC1^{Cas9}- as compared with MOC1$^{AhR\text{-}KO}$-injected mice (Fig. 1*F*) and the enhanced expression of PD-L1 on G-MDSC and DCs, CD39 on G-MDSCs and macrophages (Fig. 3), and PD1 on T cells (Fig. 2) in MOC1^{Cas9} as compared with MOC1$^{AhR\text{-}KO}$ tdLNs.

All of these AhR-mediated effects seem likely to be exacerbated by chronic IFNγ production. Consistent with previous studies (32), we noted increasing IFNγ$^+$ T cells numbers and *Ifnγ* levels in MOC1^{Cas9} tumors (Figs. 2*C*, 3*G*, and 7*A*). While IFNγ induces *Cd274* transcription (46, 48), it was surprising to find that, in the MOC1 model, much of that effect is mediated by the AhR (Fig. 7*B*). Similarly, it was striking that the well-known induction of *Ido* by IFNγ (49, 50, 57) also was predominantly AhR controlled (Fig. 7*C*). While interactions between IFNγ and AhR signaling have been suggested (58), we report here that AhR control of IFNγ-driven outcomes, specifically PD-L1 and IDO induction, can be shown in the cancer context. The findings

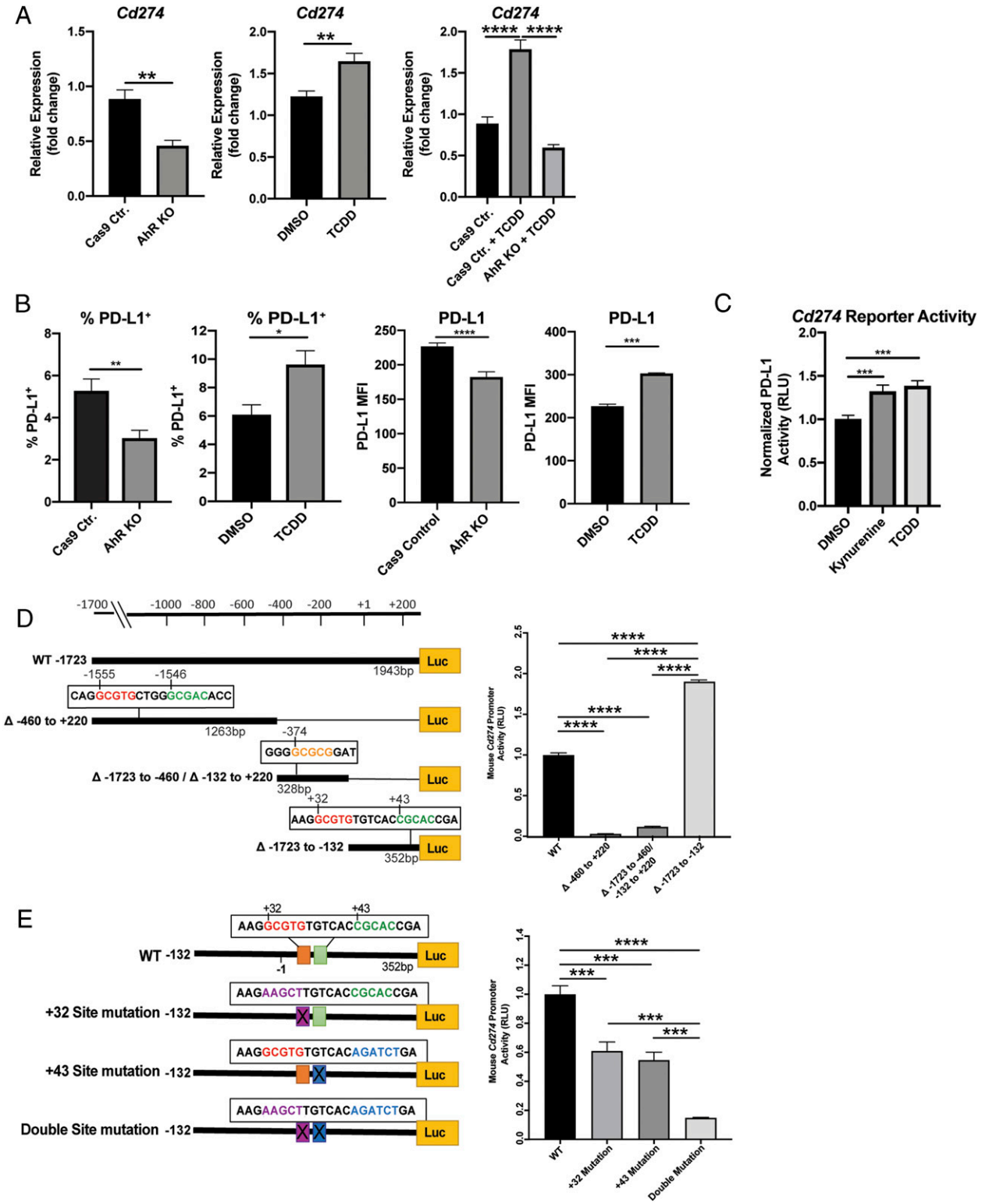

Fig. 6. The AhR regulates *Cd274*/PD-L1 expression in malignant cells. (*A*) RT-qPCR expression of *Cd274* mRNA in MOC1^{Cas9} or MOC1$^{AhR\text{-}KO}$ cells at baseline or after 24 h of treatment with TCDD (1 nM). mRNA levels in all graphs are normalized to *Gapdh* and to untreated MOC1^{WT} cells. (*B*) Percent and MFI of PD-L1 expression on MOC1^{Cas9} or MOC1$^{AhR\text{-}KO}$ at baseline or MOC1^{WT} cells 24 h after vehicle (0.1% DMSO) or TCDD (1 nM) treatment. (*C*) Normalized *Cd274* promoter activity as measured with a pGL3-Luc luciferase reporter after 24 h of treatment with kynurenine (100 μM) or TCDD (1 nM). For *A*–*C*, data are means of at least three independent experiments with three wells per group + SEM. $^{*}P < 0.05$, $^{**}P < 0.01$, $^{***}P < 0.001$ (Student's *t* test or one-way ANOVA). (*D*) The *Cd274* promoter was mutated to delete whole sections of the sequence at each of three locations containing presumptive AhR binding sites. (*E*) Normalized wild-type or AHRE-mutated *Cd274* promoter activity in MOC1 cells. The *Cd274* promoter reporter was mutated at one or both of two presumptive AhR binding sites as indicated. For *D* and *E*, data are from each one of two identical experiments presented as means + SEM, $n = 4$ wells/condition. $^{***}P < 0.001$, $^{****}P < 0.0001$ (one-way ANOVA and Tukey's multiple comparisons test).

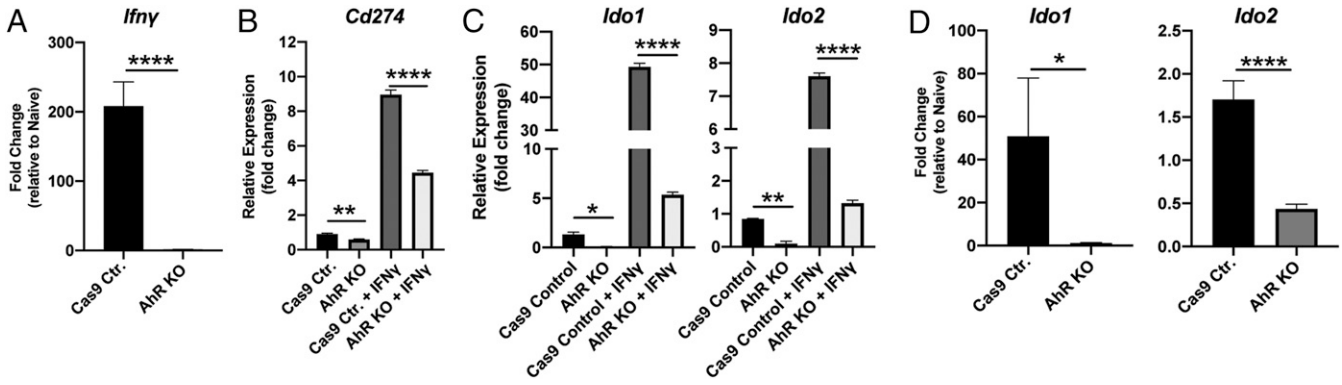

Fig. 7. IFNγ regulates *Cd274*, *Ido1*, and *Ido2* through the AhR. (*A*) RT-qPCR expression of *Ifnγ* mRNA isolated from the tongues of mice injected with MOC1^{Cas9} or MOC1$^{AhR\text{-}KO}$ cells 8 wk prior. mRNA levels were normalized to *Gapdh* and expressed relative to levels in tongues from naïve mice. Data are means + SEM, representative of three independent experiments, $n = 8$ mice/group. (*B*) RT-qPCR expression of *Cd274* mRNA in MOC1^{Cas9} or MOC1$^{AhR\text{-}KO}$ cells at baseline or after treatment with IFNγ (100 μg/mL) for 24 h. *Cd274* expression was normalized to *Gapdh* and to expression in untreated MOC1^{Cas9} cells. Data are means of three independent experiments with three wells/group + SEM. (*C*) RT-qPCR expression of *Ido1* and *Ido2* mRNA in MOC1^{Cas9} or MOC1$^{AhR\text{-}KO}$ cells left untreated or treated with IFNγ (100 μg/mL) for 24 h. Expression is normalized to *Gapdh* and relative to expression in untreated MOC1^{Cas9} cells. Data are means of three independent experiments with three wells/group + SEM. (*D*) RT-qPCR expression of *Ido1* and *Ido2* in mRNA isolated from the tongues of mice injected 70 d previously with MOC1^{Cas9} or MOC1$^{AhR\text{-}KO}$ cells. mRNA levels are normalized to *Gapdh* and expressed relative to levels in tongues from naïve mice. Data are means + SEM and are representative of three independent experiments, $n = 8$ mice/group. Throughout, $^{*}P < 0.05$, $^{**}P < 0.01$, $^{****}P < 0.0001$ (Student's *t* test or one-way ANOVA).

reflect dual roles of IFNγ in the tumor context, i.e., critical for activating acute antitumor responses yet contributing to immune evasion (59) when produced chronically. Chronic IFNγ production also may be important given the multiple other targets of IFNγ signaling in the MOC1 model (Fig. 5*E*) and in primary human OSCC (60).

Within the malignant cell itself, the AhR modulates expression of genes associated with self-renewal, invasion, metastasis, and inflammation (7, 11, 18). Here, we identified a number of AhR-regulated inflammatory signaling pathways similarly associated with cancer pathogenesis. While an IL-6 signaling module in MOC1$^{AhR\text{-}KO}$-injected tongues was higher than in MOC1^{Cas9} cells at 1 wk during the robust immune rejection of the tumor, this relationship reversed after 2 wk (Fig. 1*F*). Similarly, the IL-6 signaling pathway was significantly reduced after AhR knockout in vitro (Fig. 5*C*). These results support previous studies suggesting that the AhR regulates IL-6 expression to promote tumor growth (61–63). IL-6 is considered a biomarker of OSCC (38), especially in tobacco (i.e., environmental and chemical)-related cases (64). A role for AhR control of inflammation in the cancer context is further suggested by a decrease in IL-1 and IL-8 signaling pathways in MOC1$^{AhR\text{-}KO}$ cells (Fig. 5*C*).

AhR knockout significantly decreased chemokine (C-X-C motif) ligand mRNAs (*Cxcl2*, *Cxcl3*, and *Cxcl5*) all of which contribute to angiogenesis, migration, epithelial to mesenchymal transition (EMT), and immune evasion (65, 66). We also note that AhR knockout significantly decreased mRNAs encoding a number of genes that contribute to malignancy, including *Tnf* ($P < 0.0003$), *Muc1* ($P < 0.02$), and *Tigit* ($P < 0.00001$). These data strongly suggest a role for the AhR amplification loop specifically in malignant cell aggression and potentially in protumorigenic inflammatory responses.

Finally, these results demonstrate outcomes induced with at least tryptophan-derived endogenous ligands and, in some cases, environmental ligands like TCDD (e.g., Fig. 6). That said, other environmental or dietary AhR ligands may not generate similar outcomes, given that distinctly different effects have been seen with diverse AhR ligands in multiple contexts (37, 67).

In summary, we have identified mechanisms by which the AhR suppresses antitumor immune responses in OSCC through direct effects in malignant cells or indirect effects in the TME. The findings highlight the AhR as a critical suppressor of tumor immunity and strongly support the hypothesis that targeting the AhR is an effective approach for simultaneously inhibiting several complementary immune checkpoints especially in tumors that have been screened for AhR expression and activity, including through documentation of nuclear AhR localization or the expression of AhR biomarker genes (68, 69).

Materials and Methods

Cell Culture. MOC1 and MOC22 oral cancer cells (33) were kindly provided by R. Uppaluri, Dana Farber Cancer Institute, Boston, MA and cultured in Iscove's modified Dulbecco's media/IMDM/Ham's F-12 media containing 0.016 g/L tryptophan (Fisher Scientific). Culture details are described in *SI Appendix*.

CRISPR-Cas9-Mediated AhR Knockout. Guide RNAs targeting the mouse Ahr gene (exon 1) were designed using the Zhang laboratory web resource (https://zlab.bio/guide-design-resources) (sgRNA1, 5′-CGGCTTGCGCCGCTTGCGGC-3′; sgRNA2, 5′-AAACGTGAGTGACGGCGGGC-3′). Cell line selection and validation details are provided in *SI Appendix*.

In Vivo Experiments. Orthotopic transplants were performed as described (70). C57BL/6J or NOD/SCID mice were anesthetized and tongues gently grasped and pulled out from the mouth using forceps. Using a 1-mL syringe attached to a 27 1/2 gauge needle, 3×10^5 MOC1 or MOC22 cells were slowly injected into the right lateral side of each tongue (~1.5 mm from the tip of the tongue) so that a bulbous mass formed in the center of the tongue. Small white tumors were visible 1 wk after injection of either MOC1^{Cas9} or MOC1$^{AhR\text{-}KO}$ cells. For tongue samples taken thereafter, the entire tongue was removed by cutting the tongue at the back of the mouth and bisecting it down the middle from tip to back. Generally, the entire tongue was used for RNA isolation. In cases where histologies were done, the right half of the tongue was used for RNA and the left half for histology. For rechallenge experiments, 3×10^5 MOC1^{WT} or MOC22^{WT} cells were injected orthotopically 14, 100, or 150 d after or on the same day as orthotopic or subcutaneous (both flanks) injection of MOC1$^{AhR\text{-}KO}$ cells, as indicated in the figure legends. Tumor size was quantified using a caliper. Mouse sourcing and maintenance are detailed in *SI Appendix*.

RT-qPCR. TaqMan primer and probes sets were purchased from Applied Biosystems: *Ahr* (Mm00478930_m1), Ido1 (Mm00492590_m1), Ido2 (Mm00524210_m1), *Cd274* (Mm00452054_m1), *Ifnγ* (Mm01168134_m1), *Cyp1b1* (Mm00487229_m1), *Cyp1a1* (Mm00487218_m1), and *Gapdh* (Mm99999915_g1). See *SI Appendix* for details.

NanoString nCounter Gene Expression. Total RNA (100 ng) was isolated from MOC1$^{AhR\text{-}KO}$, MOC1^{WT}, and MOC1^{Cas9} cells from the right half (when

histologies also were done) or the entire injected tongue and analyzed using the nCounter Pan Cancer Immune Profiling Panel (NanoString Technologies) according to the manufacturer's instructions. Data were analyzed using the nSolver Analysis Software.

Transient Transfection and AhR Activity Reporter Assay. MOC1 cells were plated in a 24-well plate, allowed to adhere overnight, and cotransfected with the AhR response element-driven firefly luciferase reporter construct pGudluc (0.5 μg/mL; generously provided by M. Denison, University of California, Davis, CA) and cytomegalovirus (CMV)-green (0.25 μg/mL) using TransIT-2020 transfection reagent (Mirus). After 24 h, the cells were harvested in Glo lysis buffer (Promega). Luciferase activity was determined with the Bright-Glo luciferase system according to the manufacturer's instructions (Promega). Luminescence and fluorescence were determined using a Synergy2 multifunction plate reader (Bio-Tek). pGudluc luminescence was normalized to the CMV signal.

***Cd274* (PD-L1) Promoter Deletion and Mutagenesis.** The mouse *Cd274* promoter was kindly provided by Xiaolong Yang, Queen's University, Kingston, ON, Canada. See *SI Appendix* for details on the generation of deletion mutants.

Flow Cytometry, Western Blotting, and Scratch-Wound Assay. See *SI Appendix* for details.

In Vitro Stimulation of MOC1 Cells. For some experiments, MOC1 cells were treated with vehicle (DMSO), TCDD (1 nM, Sigma-Aldrich), FICZ (0.5 μM, Sigma-Aldrich), or kynurenine (20 μM or 100 μM Sigma-Aldrich) for 24 h.

Histology. Tongue sections were fixed in 10% formalin, embedded in paraffin, cut into 5-μ sections, and stained with hematoxylin and eosin (H&E) for imaging by light microscopy. All images were captured at the same time using the same camera settings.

Cell Counting Assay. MOC1 cells (5×10^4) were plated in triplicate in 12-well plates. Cells were harvested with trypsin at indicated timepoints and counted by hemocytometer in a 0.4% Trypan Blue solution.

Statistical Analyses. Graphs were generated and statistical analyses were performed using Prism software (GraphPad) and using the statistical tests indicated in the figure legends. Details are provided in *SI Appendix*.

Data Availability. All study data are included in the article and/or supporting information.

ACKNOWLEDGMENTS. We thank the Boston University Medical Center Flow Cytometry Core for assistance designing antibody panels. This work was supported by Grants R21 ES029624, R01 ES029136, P42 ES007381, and R01 ES025409; AnTolRx Inc.; and grants from the Find The Cause Breast Cancer Foundation, the Hahnemann Foundation, and the Diercks family.

1. F. Bray *et al*., Global cancer statistics 2018: GLOBOCAN estimates of incidence and mortality worldwide for 36 cancers in 185 countries. *CA Cancer J. Clin.* **68**, 394–424 (2018).
2. R. L. Siegel, K. D. Miller, A. Jemal, Cancer statistics, 2019. *CA Cancer J. Clin.* **69**, 7–34 (2019).
3. E. E. W. Cohen *et al*., The society for immunotherapy of cancer consensus statement on immunotherapy for the treatment of squamous cell carcinoma of the head and neck (HNSCC). *J. Immunother. Cancer* **7**, 184 (2019).
4. L. Q. M. Chow *et al*., Antitumor activity of pembrolizumab in biomarker-unselected patients with recurrent and/or metastatic head and neck squamous cell carcinoma: Results from the phase Ib KEYNOTE-012 expansion cohort. *J. Clin. Oncol.* **34**, 3838–3845 (2016).
5. Y. Z. Gu, J. B. Hogenesch, C. A. Bradfield, The PAS superfamily: Sensors of environmental and developmental signals. *Annu. Rev. Pharmacol. Toxicol.* **40**, 519–561 (2000).
6. E. A. Stanford *et al*., Role for the aryl hydrocarbon receptor and diverse ligands in oral squamous cell carcinoma migration and tumorigenesis. *Mol. Cancer Res.* **14**, 696–706 (2016).
7. B. C. DiNatale *et al*., Ah receptor antagonism represses head and neck tumor cell aggressive phenotype. *Mol. Cancer Res.* **10**, 1369–1379 (2012).
8. D. W. Kim *et al*., The RelA NF-kappaB subunit and the aryl hydrocarbon receptor (AhR) cooperate to transactivate the c-myc promoter in mammary cells. *Oncogene* **19**, 5498–5506 (2000).
9. J. J. Schlezinger *et al*., A role for the aryl hydrocarbon receptor in mammary gland tumorigenesis. *Biol. Chem.* **387**, 1175–1187 (2006).
10. X. Yang *et al*., Constitutive regulation of CYP1B1 by the aryl hydrocarbon receptor (AhR) in pre-malignant and malignant mammary tissue. *J. Cell. Biochem.* **104**, 402–417 (2008).
11. O. Novikov *et al*., An aryl hydrocarbon receptor-mediated amplification loop that enforces cell migration in ER-/PR-/Her2- human breast cancer cells. *Mol. Pharmacol.* **90**, 674–688 (2016).
12. M. Silginer *et al*., The aryl hydrocarbon receptor links integrin signaling to the TGF-β pathway. *Oncogene* **35**, 3260–3271 (2016).
13. M. C. Takenaka *et al*., Control of tumor-associated macrophages and T cells in glioblastoma via AHR and CD39. *Nat. Neurosci.* **22**, 729–740 (2019).
14. P. Lin *et al*., Overexpression of aryl hydrocarbon receptor in human lung carcinomas. *Toxicol. Pathol.* **31**, 22–30 (2003).
15. T.-L. Peng, J. Chen, W. Mao, X. Song, M.-H. Chen, Aryl hydrocarbon receptor pathway activation enhances gastric cancer cell invasiveness likely through a c-Jun-dependent induction of matrix metalloproteinase-9. *BMC Cell Biol.* **10**, 27 (2009).
16. T. Hayashibara *et al*., Possible involvement of aryl hydrocarbon receptor (AhR) in adult T-cell leukemia (ATL) leukemogenesis: Constitutive activation of AhR in ATL. *Biochem. Biophys. Res. Commun.* **300**, 128–134 (2003).
17. Z. Wang, S. Monti, D. H. Sherr, The diverse and important contributions of the AHR to cancer and cancer immunity. *Curr. Opin. Toxicol.* **2**, 93–102 (2017).
18. E. A. Stanford *et al*., The role of the aryl hydrocarbon receptor in the development of cells with the molecular and functional characteristics of cancer stem-like cells. *BMC Biol.* **14**, 20 (2016).
19. M. M. Lowe *et al*., Identification of cinnabarinic acid as a novel endogenous aryl hydrocarbon receptor ligand that drives IL-22 production. *PLoS One* **9**, e87877 (2014).
20. T. D. Hubbard *et al*., Divergent Ah receptor ligand selectivity during hominin evolution. *Mol. Biol. Evol.* **33**, 2648–2658 (2016).
21. F. J. Quintana *et al*., Control of T(reg) and T(H)17 cell differentiation by the aryl hydrocarbon receptor. *Nature* **453**, 65–71 (2008).
22. L. Apetoh *et al*., The aryl hydrocarbon receptor interacts with c-Maf to promote the differentiation of type 1 regulatory T cells induced by IL-27. *Nat. Immunol.* **11**, 854–861 (2010).
23. R. Gandhi *et al*., Activation of the aryl hydrocarbon receptor induces human type 1 regulatory T cell-like and Foxp3(+) regulatory T cells. *Nat. Immunol.* **11**, 846–853 (2010).
24. J. A. Goettel *et al*., AHR activation is protective against colitis driven by T cells in humanized mice. *Cell Rep.* **17**, 1318–1329 (2016).
25. N. T. Nguyen *et al*., Aryl hydrocarbon receptor negatively regulates dendritic cell immunogenicity via a kynurenine-dependent mechanism. *Proc. Natl. Acad. Sci. U.S.A.* **107**, 19961–19966 (2010).
26. J. Bankoti *et al*., Effects of TCDD on the fate of naive dendritic cells. *Toxicol. Sci.* **115**, 422–434 (2010).
27. J. Bankoti, B. Rase, T. Simones, D. M. Shepherd, Functional and phenotypic effects of AhR activation in inflammatory dendritic cells. *Toxicol. Appl. Pharmacol.* **246**, 18–28 (2010).
28. C. F. A. Vogel *et al*., Aryl hydrocarbon receptor signaling regulates NF-κB RelB activation during dendritic-cell differentiation. *Immunol. Cell Biol.* **91**, 568–575 (2013).
29. F. J. Quintana *et al*., An endogenous aryl hydrocarbon receptor ligand acts on dendritic cells and T cells to suppress experimental autoimmune encephalomyelitis. *Proc. Natl. Acad. Sci. U.S.A.* **107**, 20768–20773 (2010).
30. C. A. Opitz *et al*., An endogenous tumour-promoting ligand of the human aryl hydrocarbon receptor. *Nature* **478**, 197–203 (2011).
31. Y. Liu *et al*., Tumor-Repopulating cells induce PD-1 expression in $CD8^+$ T cells by transferring kynurenine and AhR activation. *Cancer Cell* **33**, 480–494.e7 (2018).
32. N. P. Judd, C. T. Allen, A. E. Winkler, R. Uppaluri, Comparative analysis of tumor-infiltrating lymphocytes in a syngeneic mouse model of oral cancer. *Otolaryngol. Head Neck Surg.* **147**, 493–500 (2012).
33. N. P. Judd *et al*., ERK1/2 regulation of CD44 modulates oral cancer aggressiveness. *Cancer Res.* **72**, 365–374 (2012).
34. P. Zolkind *et al*., Cancer immunogenomic approach to neoantigen discovery in a checkpoint blockade responsive murine model of oral cavity squamous cell carcinoma. *Oncotarget* **9**, 4109–4119 (2017).
35. G.-Z. Wang *et al*., The Aryl hydrocarbon receptor mediates tobacco-induced PD-L1 expression and is associated with response to immunotherapy. *Nat. Commun.* **10**, 1125 (2019).
36. H. Cash *et al*., mTOR and MEK1/2 inhibition differentially modulate tumor growth and the immune microenvironment in syngeneic models of oral cavity cancer. *Oncotarget* **6**, 36400–36417 (2015).
37. S. Narasimhan *et al*., Towards resolving the pro- and anti-tumor effects of the aryl hydrocarbon receptor. *Int. J. Mol. Sci.* **19**, 1388 (2018).
38. H. A. Sahibzada *et al*., Salivary IL-8, IL-6 and TNF-α as potential diagnostic biomarkers for oral cancer. *Diagnostics (Basel)* **7**, 21 (2017).
39. B. C. DiNatale, J. C. Schroeder, L. J. Francey, A. Kusnadi, G. H. Perdew, Mechanistic insights into the events that lead to synergistic induction of interleukin 6 transcription upon activation of the aryl hydrocarbon receptor and inflammatory signaling. *J. Biol. Chem.* **285**, 24388–24397 (2010).
40. J. Rotman, B. D. Koster, E. S. Jordanova, A. M. Heeren, T. D. de Gruijl, Unlocking the therapeutic potential of primary tumor-draining lymph nodes. *Cancer Immunol. Immunother.* **68**, 1681–1688 (2019).
41. A. K. D'Cruz *et al*.; Head and Neck Disease Management Group, Elective versus therapeutic neck dissection in node-negative oral cancer. *N. Engl. J. Med.* **373**, 521–529 (2015).

42. F. O. Ferreira *et al*., Association of CCL2 with lymph node metastasis and macrophage infiltration in oral cavity and lip squamous cell carcinoma. *Tumour Biol.* **29**, 114–121 (2008).
43. Z. Ling *et al*., CCL2 promotes cell migration by inducing epithelial-mesenchymal transition in oral squamous cell carcinoma. *J. Oral Pathol. Med.* **48**, 477–482 (2019).
44. L. Ding *et al*., Serum CCL2 and CCL3 as potential biomarkers for the diagnosis of oral squamous cell carcinoma. *Tumour Biol.* **35**, 10539–10546 (2014).
45. Y. G. Najjar *et al*., Myeloid-derived suppressor cell subset accumulation in renal cell carcinoma parenchyma is associated with intratumoral expression of IL1β, IL8, CXCL5, and Mip-1α. *Clin. Cancer Res.* **23**, 2346–2355 (2017).
46. A. Garcia-Diaz *et al*., Interferon receptor signaling pathways regulating PD-L1 and PD-L2 expression. *Cell Rep.* **19**, 1189–1201 (2017).
47. H. Shi *et al*., Chemokine (C-X-C motif) ligand 1 and CXCL2 produced by tumor promote the generation of monocytic myeloid-derived suppressor cells. *Cancer Sci.* **109**, 3826–3839 (2018).
48. K. Mimura *et al*., PD-L1 expression is mainly regulated by interferon gamma associated with JAK-STAT pathway in gastric cancer. *Cancer Sci.* **109**, 43–53 (2018).
49. S. A. Sarkar *et al*., Induction of indoleamine 2,3-dioxygenase by interferon-gamma in human islets. *Diabetes* **56**, 72–79 (2007).
50. M. W. Taylor, G. S. Feng, Relationship between interferon-gamma, indoleamine 2,3-dioxygenase, and tryptophan catabolism. *FASEB J.* **5**, 2516–2522 (1991).
51. C. J. Funatake, N. B. Marshall, N. I. Kerkvliet, 2,3,7,8-Tetrachlorodibenzo-p-dioxin alters the differentiation of alloreactive CD8+ T cells toward a regulatory T cell phenotype by a mechanism that is dependent on aryl hydrocarbon receptor in CD4+ T cells. *J. Immunotoxicol.* **5**, 81–91 (2008).
52. C. J. Funatake, N. B. Marshall, L. B. Steppan, D. V. Mourich, N. I. Kerkvliet, Cutting edge: activation of the aryl hydrocarbon receptor by 2,3,7,8-tetrachlorodibenzo-p-dioxin generates a population of CD4+ CD25+ cells with characteristics of regulatory T cells. *J. Immunol.* **175**, 4184–4188 (2005).
53. W. H. Neamah *et al*., AhR activation leads to massive mobilization of myeloid-derived suppressor cells with immunosuppressive activity through regulation of CXCR2 and MicroRNA miR-150-5p and miR-543-3p that target anti-inflammatory genes. *J. Immunol.* **203**, 1830–1844 (2019).
54. B. Stockinger, P. Di Meglio, M. Gialitakis, J. H. Duarte, The aryl hydrocarbon receptor: Multitasking in the immune system. *Annu. Rev. Immunol.* **32**, 403–432 (2014).
55. I. D. Mascanfroni *et al*., Metabolic control of type 1 regulatory T cell differentiation by AHR and HIF1-α. *Nat. Med.* **21**, 638–646 (2015).
56. M. C. Takenaka, S. Robson, F. J. Quintana, Regulation of the T cell response by CD39. *Trends Immunol.* **37**, 427–439 (2016).
57. T. W. Chung *et al*., Induction of indoleamine 2,3-dioxygenase (IDO) enzymatic activity contributes to interferon-gamma induced apoptosis and death receptor 5 expression in human non-small cell lung cancer cells. *Asian Pac. J. Cancer Prev.* **15**, 7995–8001 (2014).
58. Y. Liu *et al*., Blockade of IDO-kynurenine-AhR metabolic circuitry abrogates IFN-γ-induced immunologic dormancy of tumor-repopulating cells. *Nat. Commun.* **8**, 15207 (2017).
59. M. Mojic, K. Takeda, Y. Hayakawa, The dark side of IFN-γ: Its role in promoting cancer Immunoevasion. *Int. J. Mol. Sci.* **19**, 89 (2017).
60. L.-M. Chi *et al*., Enhanced interferon signaling pathway in oral cancer revealed by quantitative proteome analysis of microdissected specimens using 16O/18O labeling and integrated two-dimensional LC-ESI-MALDI tandem MS. *Mol. Cell. Proteomics* **8**, 1453–1474 (2009).
61. B. C. DiNatale, J. C. Schroeder, G. H. Perdew, Ah receptor antagonism inhibits constitutive and cytokine inducible IL6 production in head and neck tumor cell lines. *Mol. Carcinog.* **50**, 173–183 (2011).
62. B. D. Hollingshead, T. V. Beischlag, B. C. Dinatale, P. Ramadoss, G. H. Perdew, Inflammatory signaling and aryl hydrocarbon receptor mediate synergistic induction of interleukin 6 in MCF-7 cells. *Cancer Res.* **68**, 3609–3617 (2008).
63. D. Wu *et al*., Activation of aryl hydrocarbon receptor induces vascular inflammation and promotes atherosclerosis in apolipoprotein E-/- mice. *Arterioscler. Thromb. Vasc. Biol.* **31**, 1260–1267 (2011).
64. C.-H. Lee *et al*., IL-1β promotes malignant transformation and tumor aggressiveness in oral cancer. *J. Cell. Physiol.* **230**, 875–884 (2015).
65. P. J. Sarvaiya, D. Guo, I. Ulasov, P. Gabikian, M. S. Lesniak, Chemokines in tumor progression and metastasis. *Oncotarget* **4**, 2171–2185 (2013).
66. M. T. Chow, A. D. Luster, Chemokines in cancer. *Cancer Immunol. Res.* **2**, 1125–1131 (2014).
67. I. A. Murray, A. D. Patterson, G. H. Perdew, Aryl hydrocarbon receptor ligands in cancer: Friend and foe. *Nat. Rev. Cancer* **14**, 801–814 (2014).
68. Z. Wang *et al*., How the AHR became important in cancer: The role of chronically active AHR in cancer aggression. *Int. J. Mol. Sci.* **22**, 387 (2020).
69. A. Paris, N. Tardif, M.-D. Galibert, S. Corre, AhR and cancer: From gene profiling to targeted therapy. *Int. J. Mol. Sci.* **22**, 752 (2021).
70. M. V. Bais, M. Kukuruzinska, P. C. Trackman, Orthotopic non-metastatic and metastatic oral cancer mouse models. *Oral Oncol.* **51**, 476–482 (2015).